Electronic Supplementary Material (ESI) for ChemComm.

Supporting Information

Interfacial dipole engineering in all-inorganic perovskite solar cells

Kuidong Gao,[a] Lei Gao,[a] Qiurui Wang,[a] Yijie Chang,[a] Qiang Zhang, Yuanyuan Zhao,*[a] and Qunwei Tang*[b]

[a] *College of Mechanical and Electronic Engineering, Shandong University of Science and Technology, Qingdao 266590, PR China.*

[b] *Institute of Carbon Neutrality, College of Chemical and Biological Engineering, Shandong University of Science and Technology, Qingdao 266590, PR China.*

*** Corresponding Authors**. E-mail: yuanyuanzhao@sdust.edu.cn, tangqunwei@sdust.edu.cn

1. Experimental

2.1 Materials and Reagents

Stannous chloride anhydrous ($SnCl_2$, Aladdin), thiourea (CH_4N_2S, Aladdin), lead bromide ($PbBr_2$, Aladdin), cesium bromide (CsBr, Aladdin), N,N-dimethylformamide (DMF, Sinopharm), titanium tetrachloride ($TiCl_4$, Sinopharm), methanol (CH_3OH, Sinopharm), isopropanol (C_3H_8O, Sinopharm), 5-nitro-7-azaindole ($C_7H_5N_3O_2$, Acmec), 7-azaindole ($C_7H_5N_2$, Acmec), 5-methoxy-7-azaindole ($C_8H_8N_2O$), [6,6]-phenyl-C_{61}-butyric acid methyl ester ($PC_{61}BM$, Polymer), FTO glass (7 Ω square^{-1}) and carbon paste (Shanghai Mater Win New Materials Co., Ltd) were used as supplied without further purification.

2.2 Solar Cell Fabrication

The etched FTO conductive glass was ultrasonically cleaned with detergent, deionized water, and ethanol. The freshly cleaned FTO substrate was further cleaned in a plasma cleaner for 5 min. The cleaned FTO substrate and SnO_2 QDs solution were preheated at 80 °C for 5 min. The preheated SnO_2 QDs solution was spin-coated on FTO substrate at 2000 rpm for 30 s, and annealed at 200 °C for 1 h to obtain a dense SnO_2 ETL. The TiO_xCl_{4-2x} modification was performed by soaking the SnO_2 coated FTO glass in 40 mM $TiCl_4$ aqueous solution at 75 °C for 30 min, and the substrates were rinsed with deionized water and ethanol, and then dried in air at 200 °C for 30 min. Next, DMF solution of 1 M $PbBr_2$ was spin-coated on the obtained substrate (2000 rpm, 30 s) and heated at 90 °C for 30 min to obtain $PbBr_2$ film. After that, the methanol solution of 0.07 M CsBr was spin-coated (2000 rpm, 30 s) on $PbBr_2$ film surface and annealed at 250 °C for 5 min. This process was repeated for seven times until a high quality $CsPbBr_3$ film was formed. For devices with the surface passivation treatment, when the annealed perovskite films were cooled to room temperature,7-AI derivatives in isopropanol solution with different concentration was dropped

onto the perovskite films and spin-coated at 2000 rpm for 30 s and annealed at 90 °C for 15 min. At last, a conductive carbon paste was coated onto $CsPbBr_3$ layer and annealed at 90 °C for 30 min. For $CsPbI_2Br$ devices, 1.2 M $CsPbI_2Br$ precursor containing 312 mg of CsI, 277 mg of PbI_2 and 220 mg of $PbBr_2$ dissolved in 1 mL of DMSO was spin-coated onto FTO/SnO_2-TiO_xCl_{4-2x} substrate at 1000 rpm for 10 s and then at 5000 rpm for 50 s. Afterwards, the substrate was placed on a hotplate at 160 ^oC for 2 min and then at 270 ^oC for 8 min and cooled down to room temperature naturally. The remaining steps are identical to those involved in preparing $CsPbBr_3$ PSC.

2.3 Measurements and characterizations

The energy dispersive spectroscopy (EDS) mapping images were carried out using a scanning electron microscope (HORIBA EX-350). The X-ray diffraction (XRD) patterns were recorded by X-ray diffractometer (Bruker D8 Advance). Fourier transform infrared (FTIR) spectra were obtained on Fourier infrared spectrometer (Nicolet IS 10). Kelvin probe force microscopy (KPFM) images were obtained using Kelvin probe force microscopy (KPFM, CypherTM, Asylum Research). The ultraviolet photoelectron spectrometer (UPS) spectra were characterized by ultraviolet photoelectron spectroscopy (Thermo ESCALAB 250XI). A space charge limited current (SCLC) model was employed to characterize the trap density of PVK films for electron-only equipment with the structure of FTO/SnO_2-TiO_xCl_{4-2x}/$CsPbBr_3$/PCBM/carbon at the voltage range of 0-7 V under dark condition. Ultraviolet-visible (UV-vis) transmission and absorption spectra were characterized via Meipuda UV-3200 spectrophotometer. The photocurrent density-voltage (*J-V*) curves of various devices were measured by the sourcemeter of Keithley 2450 under irradiation of simulated sunlight (AM 1.5, 100 mW cm^{-2} calibrated with a standard silicon solar cell, Newport, Oriel Class A, 91195 A) at a voltage range of 0-1.7 V. The external quantum efficiency (EQE) spectra were obtained using a monochromatic incident photon-to-electron

conversion efficiency (IPCE) kit from Enli Technology Co., Ltd equipped with a standard Si crystalline solar cell as a reference. Steady power output curves at the maximum power point (MPP) were recorded by electrochemical workstation of CHI660E at the bias voltage at maximal power output point. A confocal fluorescence microscope (ISS Q2 FLIM/FFS, ISS Inc.) was employed to measure the confocal PL mapping images. The steady state photoluminescence (PL) spectra were recorded via a fluorescence spectrometer (FLS1000/FS5) excited by a 350 nm laser and the time-resolved photoluminescence (TRPL) spectra were characterized using a Horiba spectrometer with an excitation wavelength of 500 nm. Capacitance-voltage (*C*-*V*) curves were measured at a frequency of 5 kHz with an amplitude of 5 mV under dark. The dark *J*-*V* curves and the electrochemical impedance spectroscopy (EIS) of PSCs were measured on CHI660E electrochemical workstation in the dark. The open-circuit voltage (V_{oc}) decay curve was measured in open circuit mode by irradiating with 100 mW cm^{-2} light intensity for several seconds and then instantaneously switching off the light.

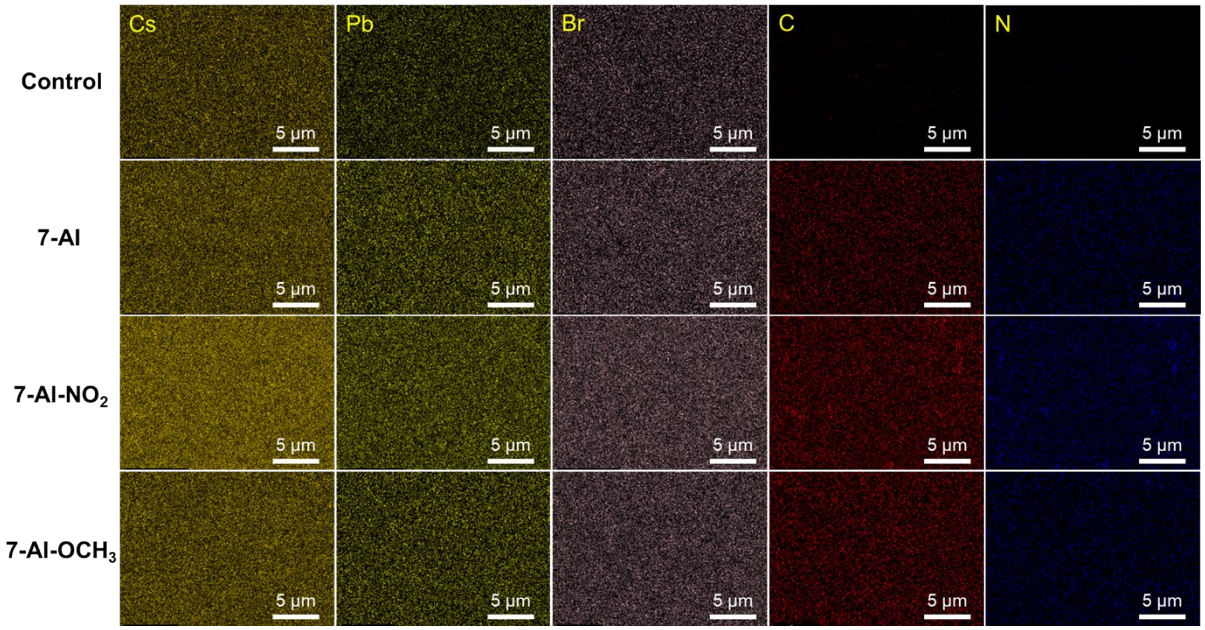

Fig. S1. The corresponding EDS mapping images of various $CsPbBr_3$ films.

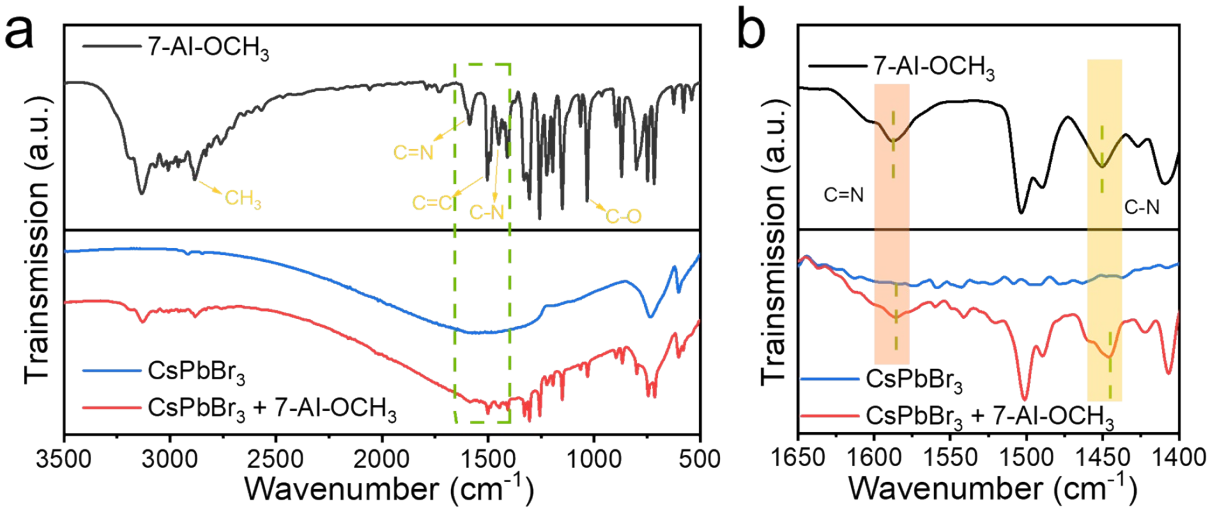

Fig. S2. (a, b) FTIR spectra of pure 7-AI-OCH_3, pure $CsPbBr_3$ perovskite, and 7-AI-OCH_3 treated $CsPbBr_3$ perovskite film.

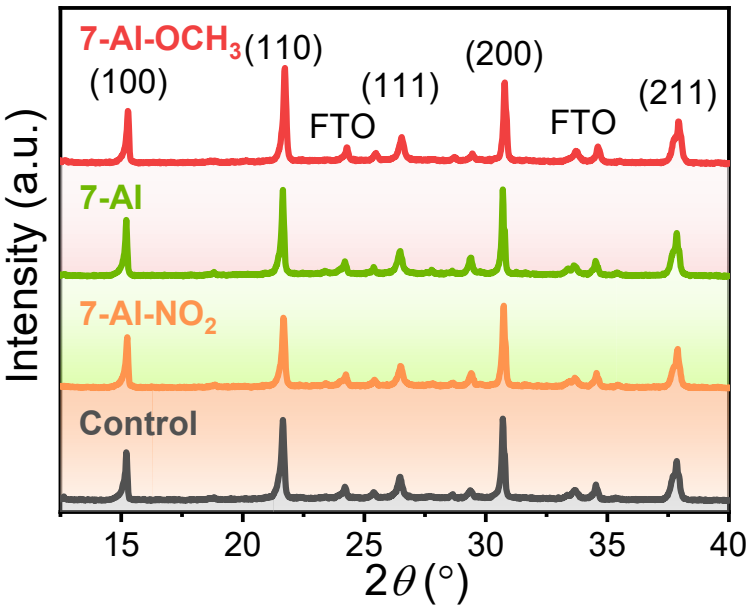

Fig. S3. XRD patterns of perovskite films with and without 7-AI derivatives treatment.

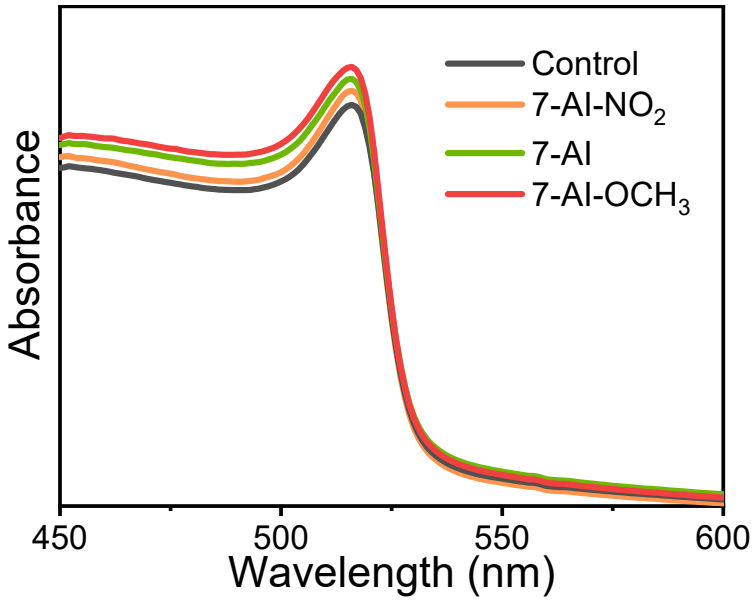

Fig. S4. UV-vis absorption spectra of various $CsPbBr_3$ films.

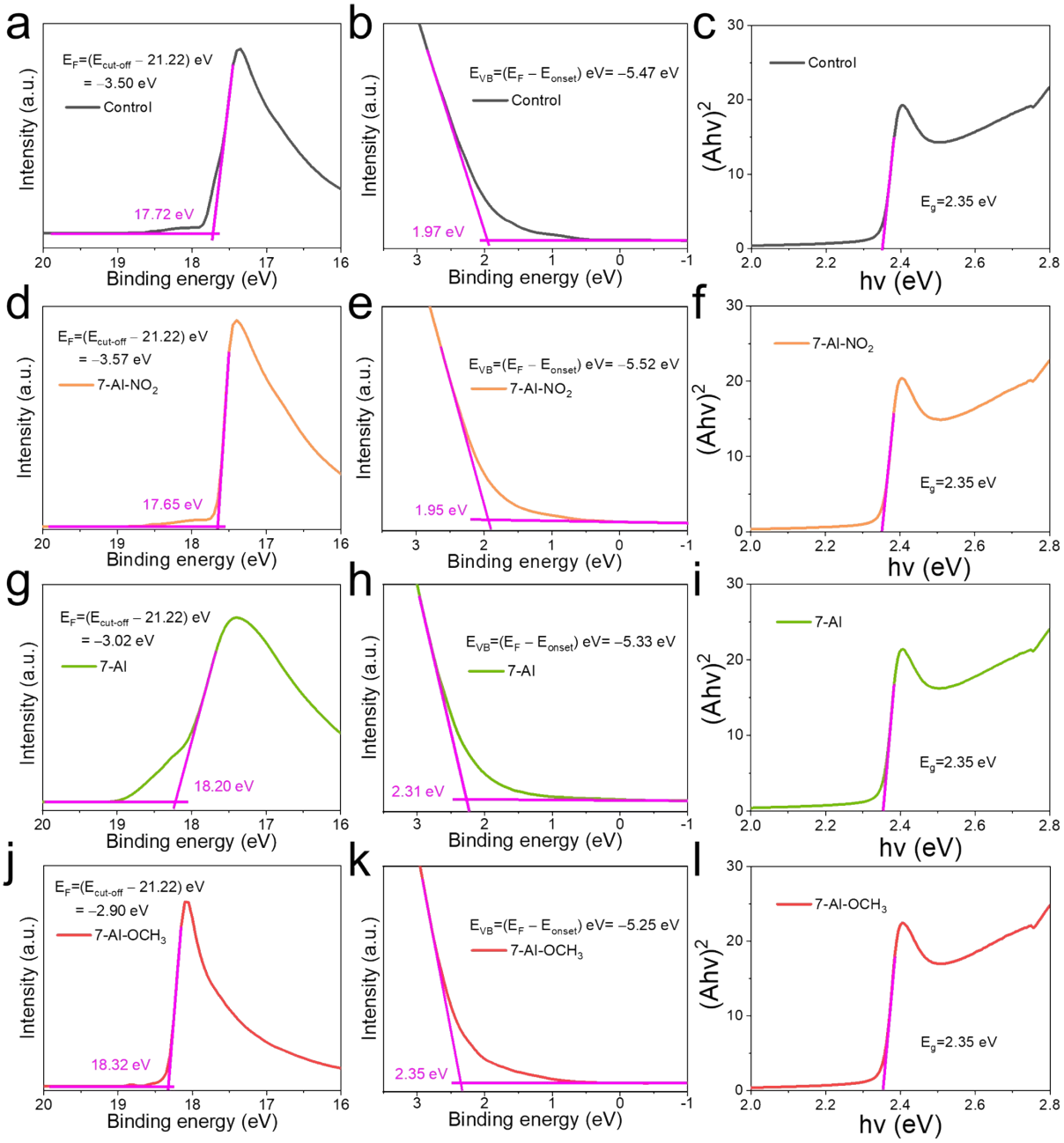

Fig. S5. UPS spectra of the (a-b) control perovskite film and the perovskite films treated with (d-e) 7-AI-NO_2, (g-h) 7-AI, (j-k) 7-AI-OCH_3. The calculation of bandgap of (c) control perovskite film and the perovskite films treated with (f) 7-AI-NO_2, (i) 7-AI, (l) 7-AI-OCH_3 dipoles.

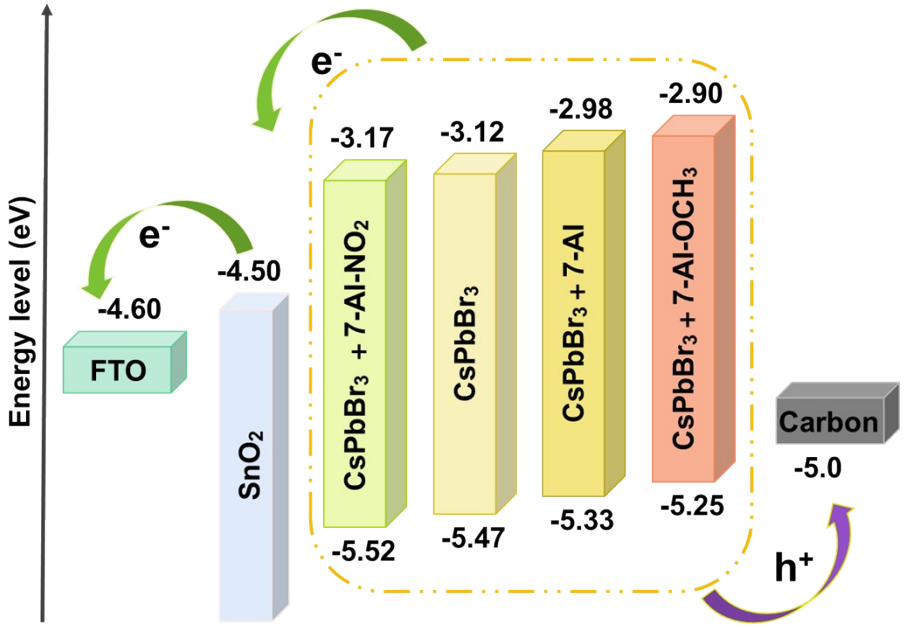

Fig. S6. The energy level schematic of the $CsPbBr_3$ PSC after treatment.

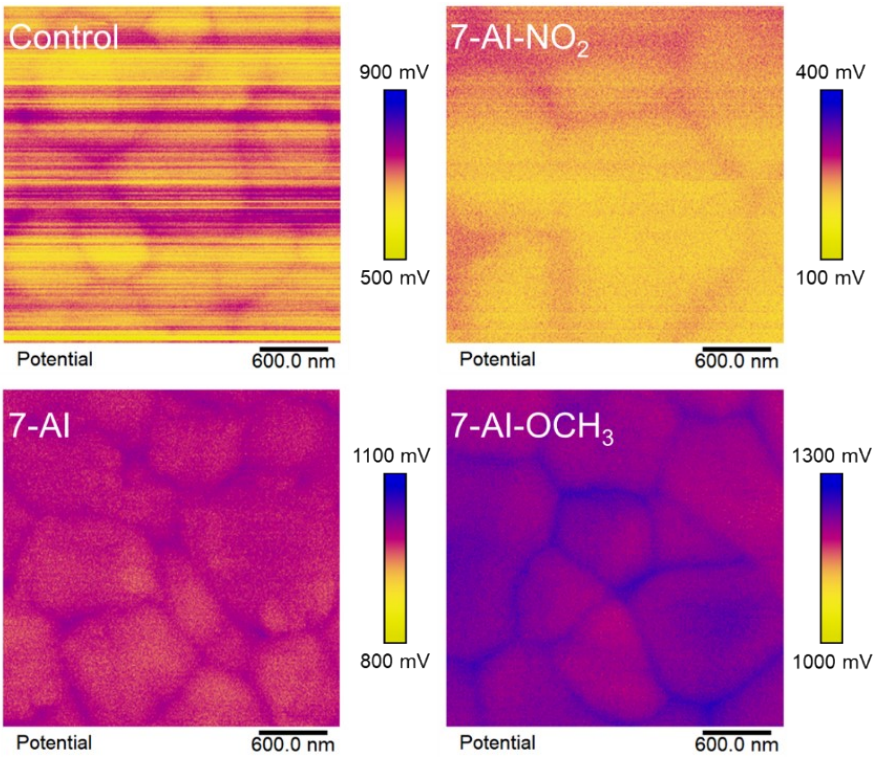

Fig. S7. The surface potential spectra for the control perovskite film and the films treated with 7-AI-NO_2, 7-AI, and 7-AI-OCH_3.

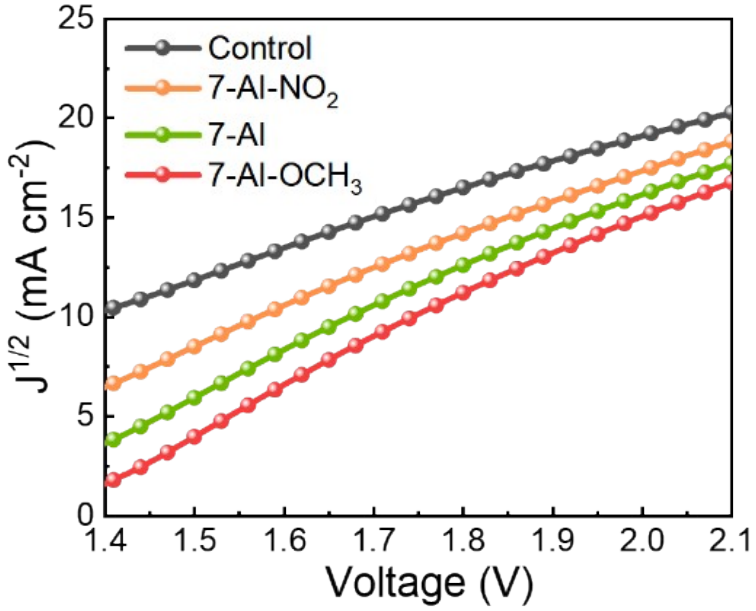

Fig. S8. The $J^{1/2}$-V curves of various devices.

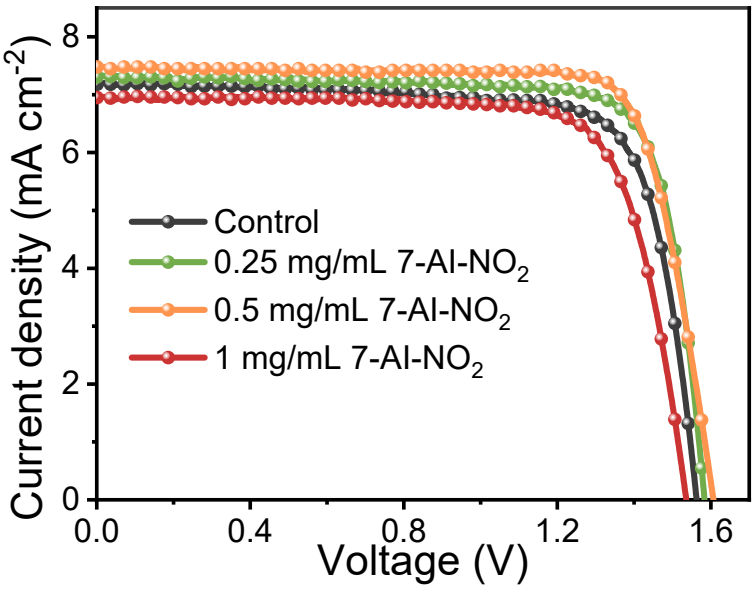

Fig. S9. *J-V* curves of the $CsPbBr_3$ PSCs fabricated with different concentrations of 7-AI-NO_2 molecules.

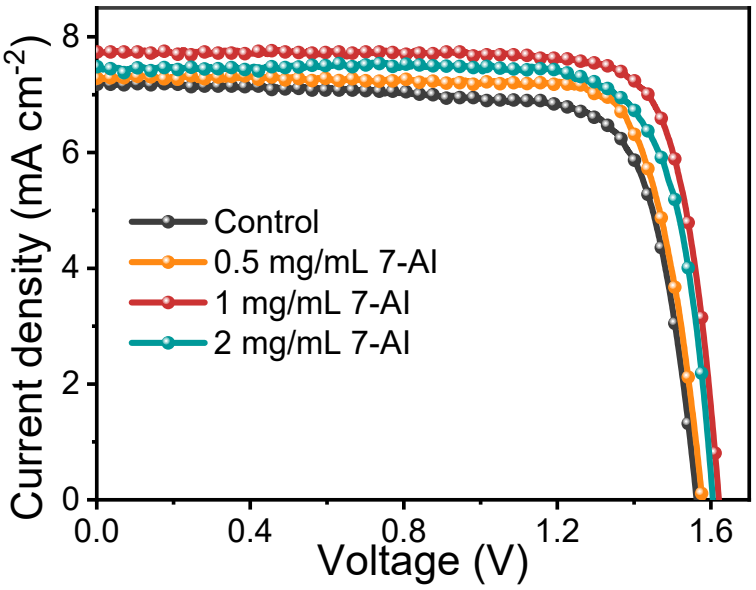

Fig. S10. *J-V* curves of the $CsPbBr_3$ PSCs fabricated with different concentrations of 7-AI molecules.

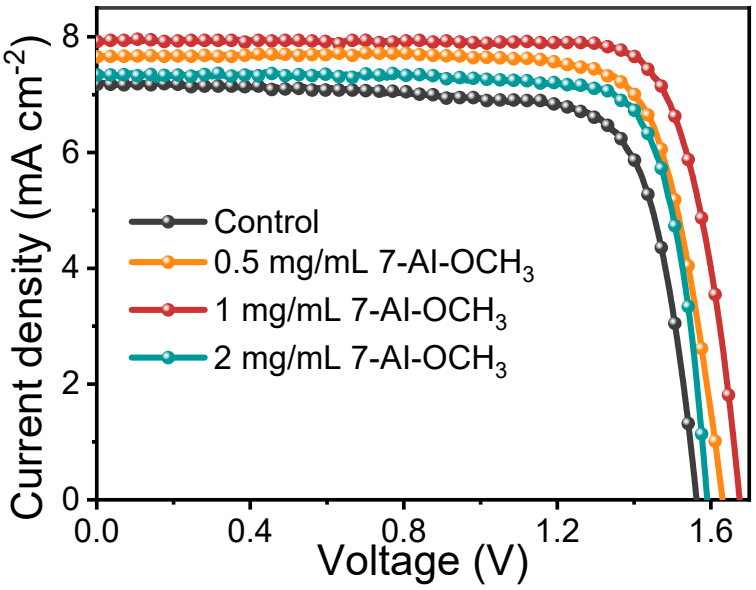

Fig. S11. *J-V* curves of the $CsPbBr_3$ PSCs fabricated with different concentrations of 7-AI-OCH_3 molecules.

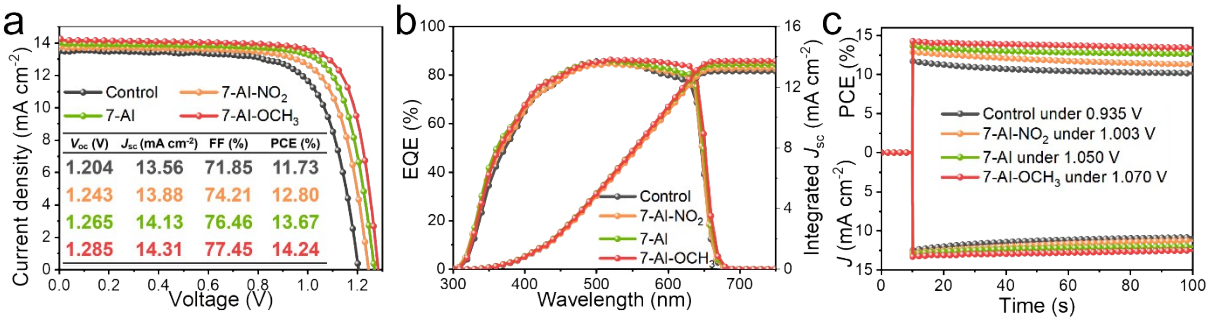

Figure S12. (a) *J-V* curves, (b) EQE spectra and (c) steady power outputs of various $CsPbI_2Br$ PSCs.

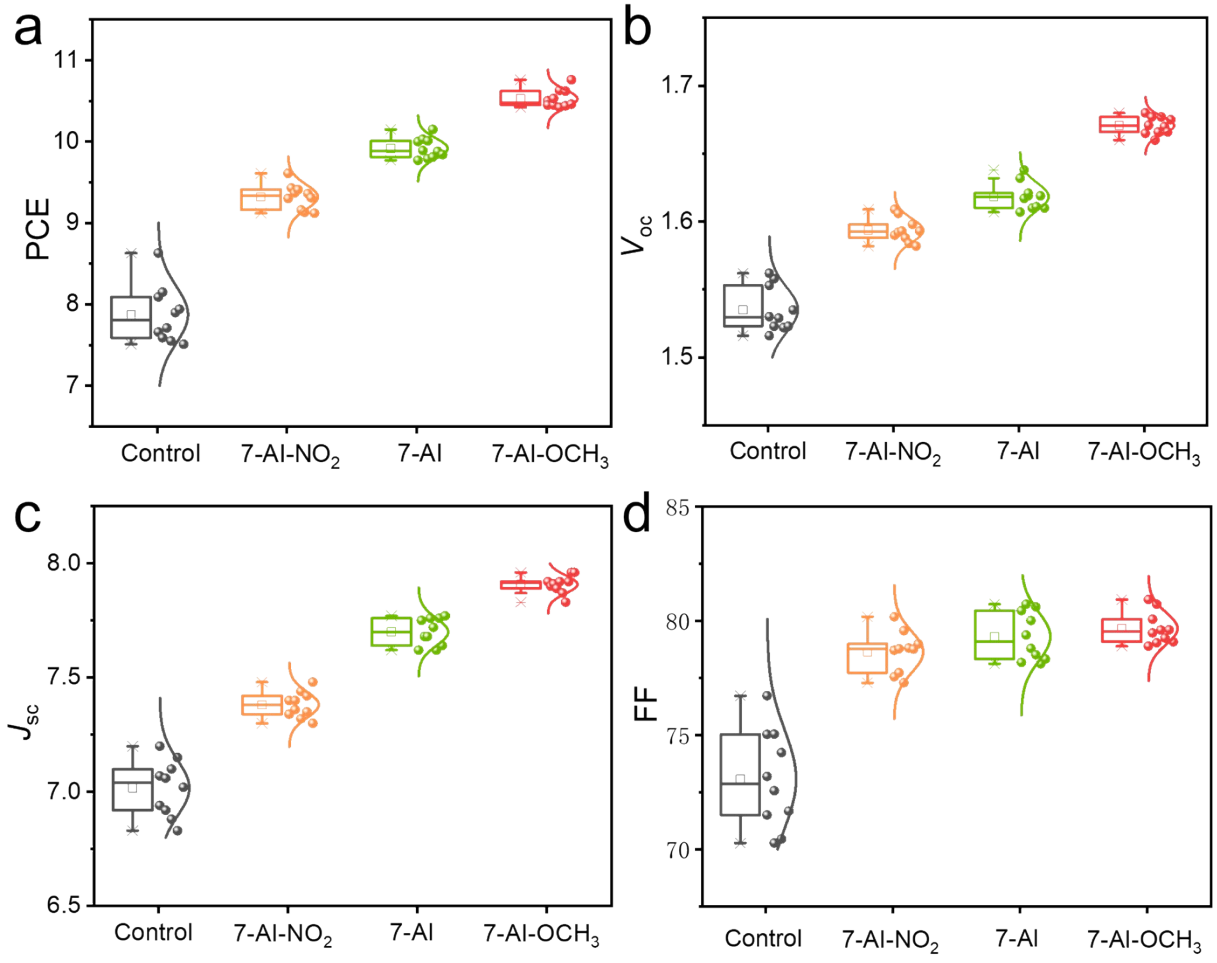

Fig. S13. (a-d) The distribution statistics of photovoltaic data (PCE, V_{oc}, J_{sc} and FF) for inorganic $CsPbBr_3$ PSCs.

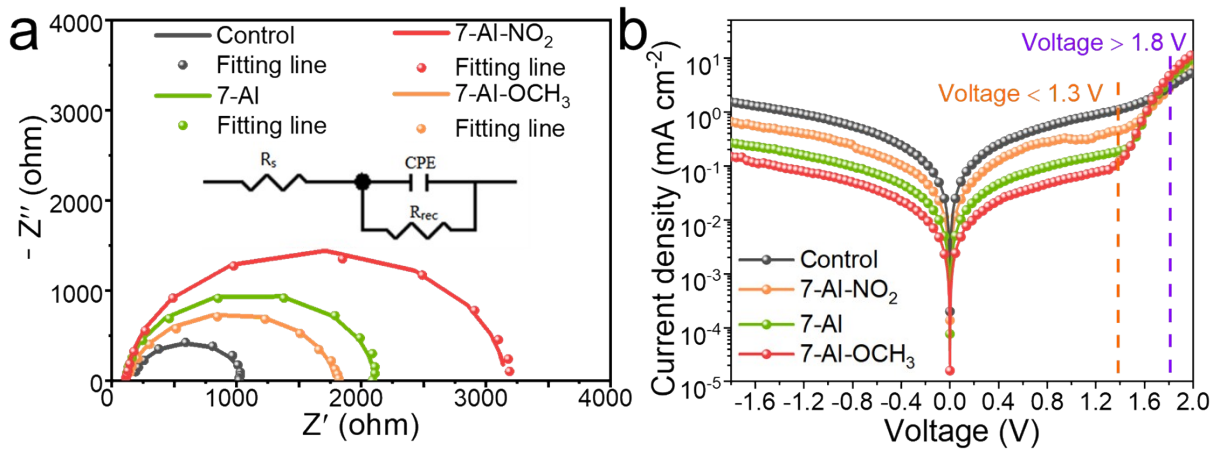

Fig. S14. (a) EIS plots and (b) the dark *J-V* curves of inorganic PSCs with control and dipole molecule tailored perovskite films.

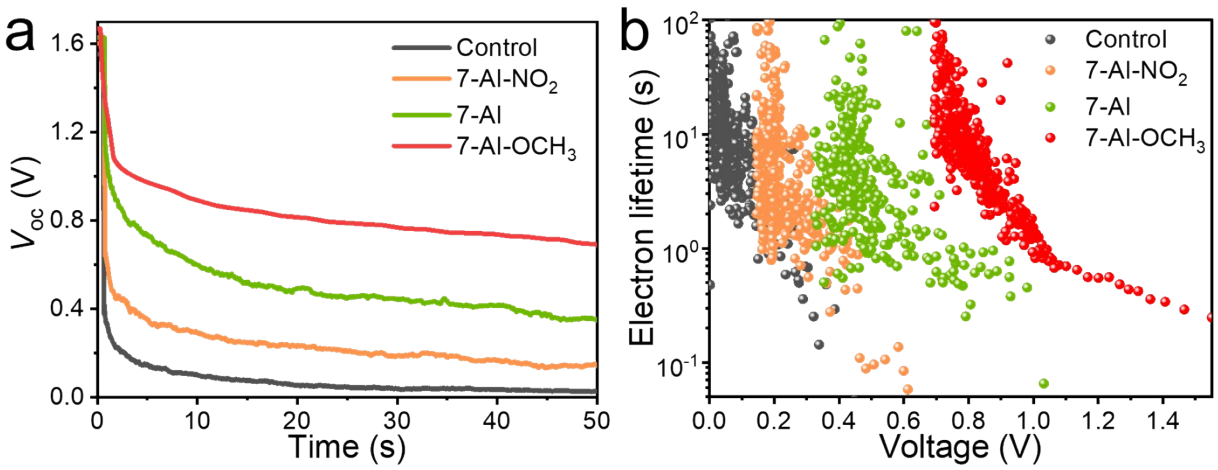

Fig. S15. (a) V_{oc} decay curves and (b) calculated electron lifetime from V_{oc} decay curves of various devices.

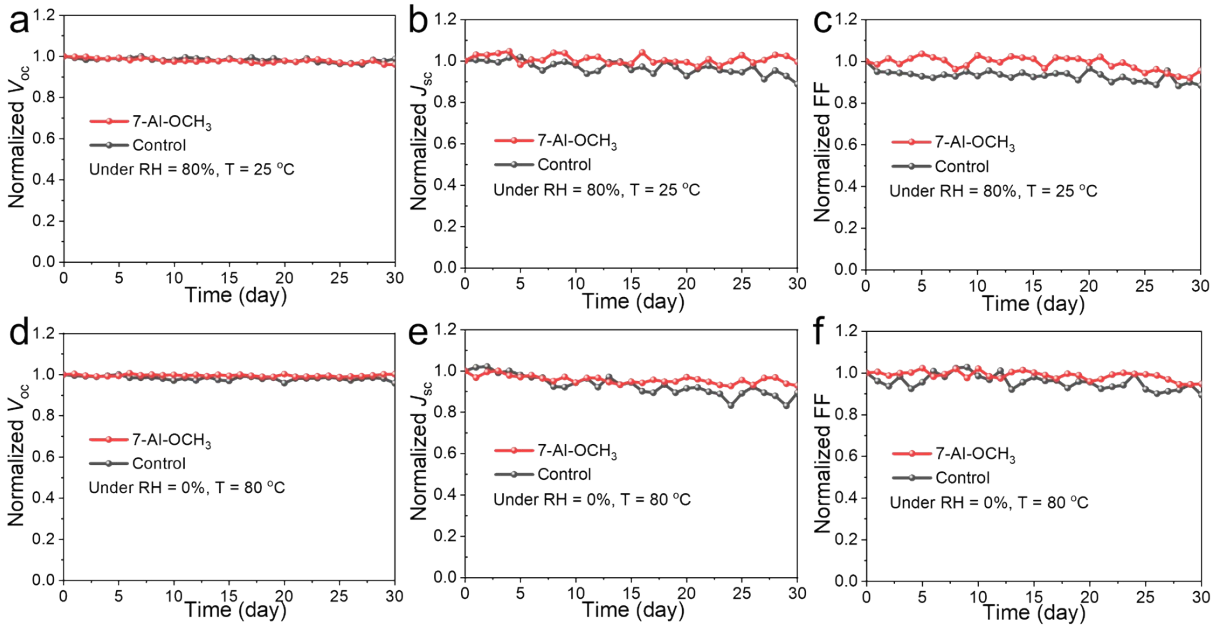

Fig. S16. The normalized parameters including V_{oc}, J_{sc} and FF of $CsPbBr_3$ PSCs at (a, b, c) RH=80%, T=25 °C and (d, e, f) RH=0%, T=80 °C.

Table S1. Photovoltaic data for state-of-the-art $CsPbBr_3$ PSCs are compared.

Devices	J_{sc} (mA cm^{-2})	V_{oc} (V)	FF (%)	PCE (%)	Ref.
Based on $CsPbBr_3$					
FTO/SnO_2-TiO_xCl_{4-2x}/$CsPbBr_3$/7-AI-OCH_3/carbon	**7.96**	**1.675**	**80.73**	**10.76**	**This work**
FTO/TiO_2/DTPT/$CsPbBr_3$/DTPT/carbon	8.52	1.574	83.67	11.21	[1]
FTO/*c*-TiO_2/*m*-TiO_2/$CsPbBr_3$/(WS_2/$AgIn_5S_8$) QDs HTM/carbon	7.49	1.627	84.03	10.24	[2]
FTO/*c*-TiO_2/*m*-TiO_2/Br-CQDs/$CsPbBr_3$-Br-CQDs/carbon	7.84	1.651	83.36	10.79	[3]
FTO/TiO_2/$CsPbBr_3$/$ReSe_2$/carbon	7.92	1.622	83.06	10.67	[4]
FTO/*c*-TiO_2/*m*-TiO_2/$CsPbBr_3$/DCC/carbon	7.79	1.611	80.96	10.16	[5]
FTO/*c*-TiO_2/*m*-TiO_2/ASF/$CsPbBr_3$/carbon	7.47	1.615	83.56	10.08	[6]
FTO/TiO_2/GQDs /$CsPbBr_3$/P3HT/carbon	9.36	1.420	73.00	9.74	[7]
FTO/*c*-TiO_2/*m*-TiO_2/$CsPbBr_3$-choline bromide/carbon	7.82	1.532	75.6	9.06	[8]
FTO/SnO_2-TiO_xCl_{4-2x}/$CsPbBr_3$+$Ti_3C_2Cl_x$/$Ti_3C_2Cl_x$/carbon	7.87	1.702	82.7	11.08	[9]
FTO/*c*-TiO_2/*m*-TiO_2/$CsPbBr_3$/Br-GO/carbon	7.88	1.602	80.01	10.10	[10]
FTO/*c*-TiO_2/*m*-TiO_2/$CsPbBr_3$/HMTA/carbon	7.51	1.605	83.63	10.08	[11]
FTO/*c*-TiO_2/*m*-TiO_2/$CsPbBr_3$:g-C_3N_4/carbon	7.80	1.278	80.25	8.00	[12]
FTO/*c*-TiO_2/*m*-TiO_2/$CsPbBr_3$/carbon	7.18	1.320	75.90	7.19	[13]
FTO/*c*-TiO_2/*m*-TiO_2/$CsPbBr_3$/$CuInS_2$/ZnS QDs/LPP-C	7.73	1.626	86.30	10.85	[14]
FTO/SnO_2/$CsPbBr_3$/N-CQDs/carbon	7.87	1.622	80.10	10.71	[15]
FTO/SnO_2-TiO_xCl_{4-2x}/WS_2/$CsPbBr_3$/carbon	7.95	1.700	79.00	10.65	[16]
FTO/SnO_2/TiO_xCl_{4-2x}/$Cs_{0.91}Rb_{0.09}PbBr_3$/carbon	7.96	1.629	80.50	10.44	[17]
FTO/*c*-TiO_2/*m*-TiO_2/AC/$CsPbBr_3$/ZnPc/carbon	7.64	1.606	82.47	10.12	[18]

FTO/TiO_2/$CsPbBr_3$/[BMMIm]Cl/carbon	7.45	1.610	83.00	9.92	[19]
FTO/*c*-TiO_2/*m*-TiO_2/$CsPbBr_3$/(MoO_2/NC)/carbon	7.20	1.532	85.20	9.40	[20]
FTO/TiO_2/$CsPbBr_3$/BHJ/carbon	7.82	1.500	76.20	8.94	[21]
FTO/*c*-TiO_2/CsBr/$CsPb_{1-x}$ Co_xBr_3/carbon	7.48	1.380	84.00	8.67	[22]
FTO/TiO_2/$CsPbBr_3$/Spiro-OMeTAD/MoO_x/ITO	7.56	1.410	73.00	7.80	[23]
FTO/*c*-TiO_2/*m*-TiO_2/$CsPbBr_3$/Cu(Cr,Ba)O_2/carbon	7.81	1.615	85.50	10.79	[24]
FTO/SnO_2/$CsPbBr_3$/$CsSnBr_3$/carbon	7.80	1.610	84.4	10.60	[25]
FTO/*c*-TiO_2/*m*-TiO_2/GQDs/$CsPbBr_3$/MnS/carbon	8.28	1.520	83.00	10.45	[26]
FTO/*c*-TiO_2/*m*-TiO_2/$Cs_{0.91}Rb_{0.09}PbBr_3$/J_{61}-ITIC/carbon	8.18	1.580	80.00	10.34	[27]
FTO/*c*-TiO_2/*m*-TiO_2/$CsPbBr_3$/P1Z1/carbon	7.652	1.578	83.06	10.03	[28]
FTO/TiO_2/$CsPbBr_3$/Ti_3C_2-MXene/carbon	8.54	1.444	73.08	9.01	[29]
FTO/*c*-TiO_2/SnO_2/$CsPbBr_3$/CuPc/carbon	8.24	1.310	81.40	8.79	[30]
FTO/*c*-TiO_2/*m*-TiO_2/$CsPb_{0.97}Tb_{0.03}Br_3$/SnS:ZnS/NiO_x/carbon	8.21	1.570	79.60	10.26	[31]
FTO/TiO_2/GQDs $CsPbBr_3$/CISZ-QDs/carbon	7.35	1.522	84.30	9.43	[32]
FTO/*c*-TiO_2/*m*-TiO_2/GQDs/$CsPbBr_3$ CdZnSe@ZnSe/carbon	7.25	1.498	79.60	8.65	[33]
FTO/*c*-TiO_2/*m*-TiO_2/$CsPbBr_3$/MoS_2 QDs/carbon	6.55	1.307	79.40	6.80	[34]

Table S2. The carrier lifetimes obtained from TRRL spectra of various $CsPbBr_3$ devices.

Samples	τ_{ave} (ns)	τ_1 (ns)	A_1 (%)	τ_2 (ns)	A_2 (%)
Control	0.649	0.649	90.81	0.649	9.19
7-AI-NO_2	0.790	0.492	67.12	1.070	32.88
7-AI	0.919	0.476	60.26	1.188	39.74
7-AI-OCH_3	1.268	0.403	69.66	1.731	30.34

The TRPL decay curves are fitted using a biexponential function of $I = Ae^{-(\tau - \tau_0)/\tau_1} + Be^{-(\tau - \tau_0)/\tau_2}$, where I is the PL intensity, τ_1 and τ_2 correspond to the fast decay time of the defect-induced non-radiative recombination and the low decay time of radiative recombination, respectively, and A_1 and A_2 are the corresponding decay constants. The average decay time (τ_{ave}) is calculated to evaluate the electron extraction ability according to $\tau_{ave} = (A_1\tau_1^2 + A_2\tau_2^2)/(A_1\tau_1 + A_2\tau_2)$.where τ_1 is the faster component of trap-mediated nonradiative recombination and τ_2 is the slower component correlated to radiative recombination.

Table S3. The V_{TFL}, N_t, and μ_h values of various $CsPbBr_3$ devices.

Samples	V_{TFL} (V)	N_t (cm^{-3})	μ_h ($cm^2\ V^{-1}\ s^{-1}$)
Control	1.402	9.478×10^{14}	2.05×10^{-3}
7-AI-NO_2	1.337	9.039×10^{14}	3.38×10^{-3}
7-AI	1.275	8.620×10^{14}	1.01×10^{-2}
7-AI-OCH_3	1.181	7.984×10^{14}	1.65×10^{-2}

The trap density (N_t) can be calculated by the following formula: $N_t = 2\varepsilon_r\varepsilon_0 V_{TFL}/qL^2$, where the ε_r value of 22 corresponds to the relative dielectric constant of the $CsPbBr_3$ film and the ε_0 value of 8.85×10^{-12} F m^{-1} represents the vacuum permittivity, q is the electron charge, L is the thickness of perovskite film, and V_{TFL}, an important factor to measure the trap states density, is the onset voltage of the trap-filled limit region.

Table S4. Energy band structure data of control, 7-AI-NO_2, 7-AI and 7-AI-OCH_3 perovskite films.

Samples	$E_{cut\text{-}off}$ (eV)	E_{onset} (eV)	E_F (eV)	VB (eV)	E_g (eV)	CB (eV)
Control	17.72	1.97	-3.50	-5.47	2.35	-3.12
7-AI-NO_2	17.65	1.95	-3.57	-5.52	2.35	-3.17
7-AI	18.20	2.31	-3.02	-5.33	2.35	-2.98
7-AI-OCH_3	18.32	2.35	-2.90	-5.25	2.35	-2.90

Table S5. The photovoltaic data for the $CsPbBr_3$ PSCs fabricated with different concentrations of 7-AI-NO_2 molecules from Fig. S9.

Devices	J_{sc} (mA cm^{-2})	V_{oc} (V)	*FF* (%)	PCE (%)
Control	1.562	7.20	76.72	8.63
0.25 mg/mL	1.583	7.33	79.61	9.24
0.5 mg/mL	1.606	7.48	79.99	9.61
1 mg/mL	1.536	6.97	76.43	8.18

Table S6. The photovoltaic data for the $CsPbBr_3$ PSCs fabricated with different concentrations of 7-AI molecules from Fig. S10.

Devices	J_{sc} (mA cm^{-2})	V_{oc} (V)	*FF* (%)	PCE (%)
Control	1.562	7.20	76.72	8.63
0.5 mg/mL	1.578	7.33	80.17	9.27
1 mg/mL	1.621	7.77	80.61	10.15
2 mg/mL	1.605	7.50	78.86	9.49

Table S7. The photovoltaic data for the $CsPbBr_3$ PSCs fabricated with different concentrations of 7-AI-OCH_3 molecules from Fig. S11.

Devices	J_{sc} (mA cm^{-2})	V_{oc} (V)	*FF* (%)	PCE (%)
Control	1.562	7.20	76.72	8.63
0.5 mg/mL	1.630	7.73	78.40	9.88
1 mg/mL	1.675	7.96	80.73	10.76
2 mg/mL	1.590	7.39	80.16	9.47

Reference

[1] Guo R, Xia J, Gu H, Chu X, Zhao Y, Meng X, et al. Effective defect passivation with a designer ionic molecule for high-efficiency vapour-deposited inorganic phase-pure $CsPbBr_3$ perovskite solar cells. J. Mater. Chem. A 2023;11:408-18.

[2] Sui H, He B, Ti J, Sun S, Jiao W, Chen H, et al. Sulfur vacancy defects healing of WS_2 quantum dots boosted hole extraction for all-inorganic perovskite solar cells. Chem. Eng. J. 2023;455:140728.

[3] Zhu J, He B, Wang M, Yao X, Huang H, Chen C, et al. Elimination of defect and strain by functionalized CQDs dual-engineering for all-inorganic HTMs-free perovskite solar cells with an ultrahigh voltage of 1.651 V. Nano Energy 2022;104:107920.

[4] Zhu J, He B, Yao X, Chen H, Duan Y, Duan J, et al. Phase control of Cs-Pb-Br derivatives to suppress 0D Cs_4PbBr_6 for high-efficiency and stable all-inorganic $CsPbBr_3$ perovskite solar cells. Small 2022;18(8):2106323.

[5] Zhu J, Liu Yu, He B, Zhang W, Cui L, Wang S et al. Efficient interface engineering of N, N'-dicyclohexylcarbodiimide for stable HTMs-free $CsPbBr_3$ perovskite solar cells with 10.16%-efficiency. Chem. Eng. J. 2022;428:131950.

[6] Cui L, He B, Ding Y, Zhu J, Yao X, Ti J, et al. Multifunctional interface modifier ammonium silicofluoride for efficient and stable all-inorganic $CsPbBr_3$ perovskite solar cells. Chem. Eng. J. 2022;431:134193.

[7] Li X, Yang M, Hou S, Yan J, Dong J, Zou L, et al. Dual interfacial modification to improve the performance of $CsPbBr_3$ perovskite solar cells. Mater. Sci. Semicond Process 2022;141:106450.

[8] Cui C, Li C, Liu W, Liu Y, Niu S, Xu Z, et al. Rational Design on chemical regulation of

interfacial microstress engineering by matching young's modulus in a $CsPbBr_3$ perovskite film with mechanical compatibility toward enhanced photoelectric conversion efficiency. ACS Appl. Mater. Interfaces 2022;14(17):20257-67.

[9] Zhou Q, Duan J, Du J, Guo Q, Zhang Q, Yang X, et al. Tailored lattice "tape" to confine tensile interface for 11.08%-efficiency all-inorganic $CsPbBr_3$ perovskite solar cell with an ultrahigh voltage of 1.702 V. Adv. Sci. 2021;8(19):2101418.

[10] Sun X, He B, Zhu J, Zhu R, Chen H, Duan Y, et al. Multifunctional brominated graphene oxide boosted charge extraction for high-efficiency and stable all-inorganic $CsPbBr_3$ perovskite solar cells. Chem. Eng. J. 2021;412:128727.

[11] Sun M, Zhu J, He B, Bu F, Ti J, Yao X, et al. Efficient defect passivation and charge extraction with hexamethylenetetramine interface modification for hole-transporting layers-free $CsPbBr_3$ perovskite solar cells. Sol. RRL 2021;5(8):2100344.

[12] Liu W, Liu Y, Cui C, Niu S, Niu W, Liu M, et al. All-inorganic $CsPbBr_3$ perovskite solar cells with enhanced efficiency by exploiting lone pair electrons via passivation of crystal boundary using carbon nitride (g-C_3N_4) nanosheets. Mater. Today Energy 2021;21:100782.

[13] Ding X, Zhang Y, Sheng F, Li Y, Zhi L, Cao X, et al. Preparation of $CsPbBr_3$ films for efficient perovskite solar cells from aqueous solutions. ACS Appl. Energy Mater. 2021;4(6):5504-10.

[14] Duan J, Wang Y, Yang X, Tang Q. Alkyl-chain-regulated charge transfer in fluorescent inorganic $CsPbBr_3$ perovskite solar cells. Angew. Chem. Int. Ed. 2020;59(11):4391-5.

[15] Zhao Y, Duan J, Wang Y, Yang X, Tang Q. Precise stress control of inorganic perovskite films for carbon-based solar cells with an ultrahigh voltage of 1.622 V. Nano Energy 2020;67:104286.

[16] Zhou Q, Duan J, Yang X, Duan Y, Tang Q. Interfacial strain release from the $WS_2/CsPbBr_3$ van der waals heterostructure for 1.7 V voltage all-inorganic perovskite solar cells. Angew. Chem. Int. Ed. 2020;59(49):21997-2001.

[17] Zhou Q, Duan J, Wang Y, Yang X, Tang Q. Tri-functionalized TiO_xCl_{4-2x} accessory layer to boost efficiency of hole-free, all-inorganic perovskite solar cells. J. Energy Chem. 2020;50:1-8.

[18] Zhu J, Tang M, He B, Zhang W, Li X, Gong Z, et al. Improved charge extraction through interface engineering for 10.12% efficiency and stable $CsPbBr_3$ perovskite solar cells. J. Mater. Chem. A 2020;8:20987-97.

[19] Zhang W, Liu X, He B, Gong Z, Zhu J, Ding Y, et al. Interface engineering of imidazolium ionic liquids toward efficient and stable $CsPbBr_3$ perovskite solar cells. ACS Appl. Mater. Interfaces 2020;12(4):4540-8.

[20] Zong Z, He B, Zhu J, Ding Y, Zhang W, Duan J, et al. Boosted hole extraction in all-inorganic $CsPbBr_3$ perovskite solar cells by interface engineering using MoO_2/N-doped carbon nanospheres composite. Sol. Energy Mater. Sol. Cells 2020;209:110460.

[21] Du J, Duan J, Duan Y, Tang Q. Tailoring organic bulk-heterojunction for charge extraction and spectral absorption in $CsPbBr_3$ perovskite solar cells. Sci. China Mater. 2020;64:798-807.

[22] Wang C, Long Y, Liu X, Fu S, Wang J, Zhang J, et al. A dual promotion strategy of interface modification and ion doping for efficient and stable carbon-based planar $CsPbBr_3$ perovskite solar cells. J. Mater. Chem. C 2020;8:17211-21.

[23] Ren Y, Hao Y, Zhang N, Arain Z, Mateen M, Sun Y, et al. Exploration of polymer-assisted crystallization kinetics in $CsPbBr_3$ all-inorganic solar cell. Chem. Eng. J. 2020;392:123805.

[24] Duan J, Zhao Y, Wang Y, Yang X, Tang Q. Hole-boosted Cu(Cr,M)O_2 nanocrystals for all-inorganic $CsPbBr_3$ perovskite solar cells. Angew. Chem. Int. Ed. 2019;58(45):16147-51.

[25] Zhao Y, Duan J, Yuan H, Wang Y, Yang X, He B, et al. Using SnO_2 QDs and $CsMBr_3$ (M = Sn, Bi, Cu) QDs as charge-transporting materials for 10.6%-efficiency all-inorganic $CsPbBr_3$ perovskite solar cells with an ultrahigh open-circuit voltage of 1.610 V. Sol. RRL 2019;3(3):1800284.

[26] Li X, Tan Y, Lai H, Li S, Chen Y, Li S, et al. All-inorganic $CsPbBr_3$ perovskite solar cells with 10.45% efficiency by evaporation-assisted deposition and setting intermediate energy levels. ACS Appl. Mater. Interfaces 2019;11(33):29746-52.

[27] Zhao Y, Xu H, Wang Y, Yang X, Duan J, Tang Q. 10.34%-efficient integrated $CsPbBr_3$/bulk-heterojunction solar cells. J. Power Sources 2019;440:227151.

[28] Liu Y, He B, Duan J, Zhao Y, Ding Y, Tang M, et al. Poly(3-hexylthiophene)/zinc phthalocyanine composites for advanced interface engineering of 10.03%-efficiency $CsPbBr_3$ perovskite solar cells. J. Mater. Chem. A 2019;7:12635-44.

[29] Chen T, Tong G, Xu E, Li H, Li P, Zhu Z, et al. Accelerating hole extraction by inserting 2D Ti_3C_2-MXene interlayer to all inorganic perovskite solar cells with long-term stability. J. Mater. Chem. A 2019;7:20597-603.

[30] Liu X, Tan X, Liu Z, Ye H, Sun B, Shi T, et al. Boosting the efficiency of carbon-based planar $CsPbBr_3$ perovskite solar cells by a modified multistep spin-coating technique and interface engineering. Nano Energy 2019;56:184-95.

[31] Yuan H, Zhao Y, Duan J, Wang Y, Yang X, Tang Q. All-inorganic $CsPbBr_3$ perovskite solar cell with 10.26% efficiency by spectra engineering. J. Mater. Chem. A 2018;6:24324-9.

[32] Duan J, Hu T, Zhao Y, He B, Tang Q. Carbon-electrode-tailored all-inorganic perovskite

solar cells to harvest solar and water-vapor energy. Angew. Chem. Int. Ed. 2018;57(20):5746-9.

[33] Li Q, Bai J, Zhang T, Nie C, Duan J, Tang Q. CdZnSe@ZnSe colloid alloy quantum dots for high-efficiency allinorganic perovskite solar cells. Chem. Commun. 2018;54:9575-8.

[34] Duan J, Dou D, Zhao Y, Wang Y, Yang X, Yuan H, et al. Spray-assisted deposition of $CsPbBr_3$ films in ambient air for large-area inorganic perovskite solar cells. Mater. Today Energy 2018;10:146-52.